

The Galactic Branches as a Possible Evidence for Transient Spiral Arms

Angeles Pérez-Villegas^{1,2} *, Gilberto C. Gómez¹ † and Bárbara Pichardo³ ‡

¹ Centro de Radioastronomía y Astrofísica, Universidad Nacional Autónoma de México, Apdo. postal 3-72, Morelia Mich. 58089, México

² Max-Planck-Institut für Extraterrestrische Physik, Gießenbachstraße, D-85741 Garching, Germany

³ Instituto de Astronomía, Universidad Nacional Autónoma de México, Apdo. postal 70-264 Ciudad Universitaria, D.F. 04510, México

Accepted . Received ; in original form

ABSTRACT

With the use of a background Milky-Way-like potential model, we performed stellar orbital and magnetohydrodynamic (MHD) simulations. As a first experiment, we studied the gaseous response to a bisymmetric spiral arm potential: the widely employed cosine potential model and a self-gravitating tridimensional density distribution based model called PERLAS. Important differences are noticeable in these simulations, while the simplified cosine potential produces two spiral arms for all cases, the more realistic density based model produces a response of four spiral arms on the gaseous disk, except for weak arms -i.e. close to the linear regime- where a two-armed structure is formed. In order to compare the stellar and gas response to the spiral arms, we have also included a detailed periodic orbit study and explored different structural parameters within observational uncertainties. The four armed response has been explained as the result of ultra harmonic resonances, or as shocks with the massive bisymmetric spiral structure, among other. From the results of this work, and comparing the stellar and gaseous responses, we tracked down an alternative explanation to the formation of branches, based only on the orbital response to a self-gravitating spiral arms model. The presence of features such as branches, might be an indication of transiency of the arms.

Key words: MHD – Galaxy: disc – Galaxy: structure – Galaxy: kinematics and dynamics – galaxies: spiral – galaxies: structure

1 INTRODUCTION

Spiral arms are one of the the most striking, beautiful and scientifically challenging structures of

disc galaxies. They have fascinated and intrigued astronomers for centuries. As a rough initial approximation to treat this complex problem, the spiral arms had to be assumed as almost massless and/or with extremely modest pitch angles, in order to obtain a solution as a linear perturbation to the axisymmetric background potential. The proposed solution to the permanence of spi-

* E-mail: a.perez@crya.unam.mx

† E-mail: g.gomez@crya.unam.mx

‡ E-mail: barbara@astro.unam.mx

ral arms in galaxies was based on the spiral density wave linear theory (Lin & Shu 1964, inspired in the 60's work of B. Lindblad and P.O. Lindblad). The analytical solution at first order of the theory, known as the tight-winding approximation (TWA), that represents a weak potential model, extremely idealized as a smooth, even negligible perturbation to the background potential, was modeled as a simplified cosine function to represent the spiral arms gravitational potential. Probably followed by this initial attempt of solving the nature of spiral arms, a lot of work has tackled repeatedly the problem of modeling them, as a simplified periodic function that disregards the importance of their dynamical effects. However, spiral arms have proven to be an influential feature on galactic modern models (such as PERLAS and N-body models, based on three dimensional density structures), far beyond of a simple smooth perturbation.

If we compare the spiral arms with the galactic bar, the latter has a mass between 10 and 20% of the disc mass (Matsumoto et al. 1982; Dwek et al. 1995; Zhao 1996; Weiner & Selwood 1999), unlike the spiral arms that have a mass smaller in general than 5% of the disc mass (Pichardo et al. 2003). Consequently, the largest influence on the disc of strongly barred galaxies is, of course, due to the central bar. Therefore one would be tempted to oversimplify the scenario, by assuming that spiral arms are not influential at all on the dynamics of the disc. However, there are determinations that suggest that the majority of spiral galaxies, or at least those with clearly delineated spiral arms, are rather far from being linear (Antoja et al. 2011; Antoja et al. 2010; Antoja et al. 2009; Voglis et al. 2006; Roca-Fàbrega et al. 2013, 2014; Pichardo et al. 2003; Kawata et al. 2014; Sellwood & Carlberg 2014; Sellwood 2011).

Based on all those rigorous studies, spiral arms seem to merit an extra effort to model them beyond a simple perturbing term. This fact is even more significant in the case of the interstellar gas, which is considerably more sensitive to the details of the potential, and in general, responds strongly even if the mass of the spiral arms is only a small fraction of the axisymmetric background (Kim et al. 2014; Gómez et al. 2013; Shu et al. 1973).

For almost a century, formal studies of spiral arms have been carried on. Yet, the spiral arms morphology, origin and na-

ture are still poorly understood. With respect to their morphology, there is plentiful theoretical and observational literature on structures related to spiral arms, such as spurs, branches, feathers and beads, and their plausible explanations (Weaver 1970; Lynds 1970; Shu et al. 1973; Sofue 1976; Elmegreen 1980; Scoville et al. 2001; Lee & Shu 2012; Kim & Ostriker 2006; Chakrabarti et al. 2003; Kim & Ostriker 2002; Dobbs et al. 2011; Shetty & Ostriker 2006; Corder et al. 2008; Balbus 1988). Regarding spurs and feathering, interesting scenarios to explain these features include plain hydrodynamic simulations, where the Kelvin-Helmholtz instability creates spurs produced by shocks with the spiral arms (Wada & Koda 2004; an extension to self-gravitating three dimensional models of this work is presented in Kim & Ostriker 2006). Other scenarios include the use of global MHD simulations, adding gas self-gravity and magnetic fields that produce differential compression of gas flowing through the arms resulting in the formation of sheared structures in the interarm regions that resemble spurs and feathers (Shetty & Ostriker 2006; Kim & Ostriker 2002), or through gravitational or magneto-Jeans instabilities (Balbus 1988).

On the other hand, features such as branches are significantly longer than spurs that emerge almost parallel to the main spiral arms but with different pitch angles (usually smaller), and are generally associated with resonances. It is worth to note that, in the literature, the names spurs, feathers and branches are assigned to slightly different structures. In this work we will adopt the definition given by Feitzinger & Schwerdtfeger (1982) and Chakrabarti et al. (2003), where the “spurs” and “feathers” are small structures that arise almost perpendicularly from the main spiral arm, and “branches” are narrow structures that arise almost parallel to the main spiral arm, with smaller pitch angles and extension longer than spurs (examples of branches can be seen in galaxies like NGC 309, NGC 1637, NGC 2997, NGC 6946, among others). Regarding such structures, theory and

gas simulations have already shown a bifurcation of spiral arms produced by ultraharmonic resonances induced by the main spiral arm on the background gas flow (Shu et al. 1973; Patsis et al. 1994, 1997; Chakrabarti et al. 2003; Artymowicz & Lubow 1992). In this case, the bifurcation of the arms is expected due to the topology of the stable periodic orbits at the 4/1 resonance. Other interpretations also include the possibility that branches are the response of the gas produced by strong shocks against the main massive spiral arms, i.e. the ones made mainly of older and smaller stars (Fujimoto 1968; Roberts 1969; Shu et al. 1973; Barbanis & Woltjer 1967; Roberts, Huntley & van Albada 1979; Martos et al. 2004; Kim & Kim 2014; Chakrabarti et al. 2003; Yañez et al. 2008).

Specifically, regarding the Milky Way Galaxy, its general structure has been extensively studied and the latest determinations seem to agree with two grand design symmetric spiral arms, seen on IR and optical, and some other weaker arms, detectable mainly in optical observations (Drimmel & Spergel 2001; Benjamin et al. 2005; Drimmel 2000; Drimmel & Spergel 2001; Vallée 2013, 2002). The weaker arms (**branches**) have been explained through hydrodynamic simulations as the response to the two-armed stellar pattern. For example, Englmaier & Gerhard (1999) and Fux (1999) found that the gas response to a barred potential can produce a four-armed spiral structure. Likewise, from hydrodynamic and magnetohydrodynamic (MHD) simulations, the gas responds to an imposed two-armed spiral potential with four spiral arms (Gómez et al. 2013; Martos et al. 2004; Shu et al. 1973). In this context, the gas component shocks at the position of the spiral arms, producing a density enhancement and star formation (Fujimoto 1968; Roberts 1969; Moore et al. 2012; Seo & Kim 2014) that, depending on the relative velocity between the gas and the spiral arm, dwell upstream or downstream or in the spiral arm. In particular, Roberts (1969) showed that the nonlinear response of the gas to a stationary stellar spiral arm potential may produce two shocks, which then would be associated to a doubling of the spiral arm number as seen in the

gas component. Shu et al. (1973) demonstrated that shocks in galaxies arise necessarily if the spiral arm strength exceeds a certain critical value. Additionally, they found a range of values for the wave frequency that generates an ultraharmonic resonance which can provoke a secondary compression of the interstellar gas. This effect has been related to the origin of the Carina arm in the Milky Way (Shu et al. 1973), for example. However, since branches have been traditionally explained as shocks induced by the spiral arms, it is important to mention other observational work that shows there is little difference (or non at all) in the star formation efficiency (i.e. no shocks) between the spiral arms regions and the rest of the disk (Foyle et al. 2010; Eden et al. 2013; Foyle et al. 2011; Dobbs et al. 2011).

Finally, regarding their nature, a problem of great interest is whether spiral arms are a transient or a long-lived feature. On this matter, recent numerical simulations show that spiral arms are transient and recurrent structures (Dobbs & Bonnell 2006; Wada et al. 2011; Roškar et al. 2012; D’Onghia et al. 2013; Pérez-Villegas et al. 2013, 2012; Sellwood 2011; Sellwood & Carlberg 2014; Kawata et al. 2014; Foyle et al. 2011). However, in a study by Scarano & Lépine (2013) on a sample of 27 galaxies, the authors concluded that the break found in the radial metallicity distribution near to corotation resonance (CR), implies that the spiral structure is a rather long lived feature. Other authors, employing different techniques, seem to find observational proofs of long-lasting spiral arms (Martínez-García & González-Lópezlira 2013; Donner & Thomasson 1994; Zhang 1998).

In this work we explore the gas response to a bisymmetric spiral arm potential. For this purpose we employed two different models, a cosine potential (generally used in literature) and the three-dimensional, density distribution based potential PERLAS, applied to the particular case of a Milky Way-like galaxy. With this study we find an alternative explanation to the formation of branches in disk galaxies, and their relation to transient or long-lived spiral arms.

This paper is organized as follows. In Section 2, the galactic potential used to compute the stellar orbits and the MHD initial simulation setup are described. In Section 3, we present first a comparison between the models of the spiral arms: PERLAS and the cosine potential; second,

we present the gas response to spiral arms PERLAS model changing the structural parameters such as the pitch angle and the mass of the spiral arms, and their connection with the presence of galactic branches as a signature of transient spiral arms. Finally, we present a discussion and our conclusions in Section 4.

2 METHODOLOGY AND NUMERICAL IMPLEMENTATION

Motivated by the fact that the gas in galaxies is dynamically colder than the stellar disk, in addition to being collisional, we can expect it to be much more sensitive to details of the given potential than stars. Therefore, any differences between the cosine and PERLAS potentials might be magnified in gas with respect to the stellar response. **And so**, for purposes of comparison, we produce the whole study employing both potentials. In this section we introduce briefly the cosine and PERLAS potential models and the MHD setup applied to a Milky Way like Galaxy.

In all cases, the spiral arm models are superimposed to the axisymmetric background potential of Allen & Santillán (1991), which includes a Miyamoto-Nagai bulge and disk, and a supermassive spherical halo. Table 1 presents the basic parameters of the axisymmetric background potential.

2.1 Spiral arm models

2.1.1 Cosine Potential

As mentioned before, a large majority of the investigations on the gas associated to spiral arms model them as a linear perturbation of the axisymmetric background, represented by

$$\Phi_{sp}(R, \phi) = f(R) \cos[2\phi + g(R)], \quad (1)$$

where R, ϕ are cylindrical coordinates, $f(R)$ is the amplitude function of the perturbation, given by Contopoulos & Grosbøl (1986) as $f(R) = -ARe^{\epsilon_s R}$, where A is the amplitude and ϵ_s is the inverse of the scale-length. Finally, $g(R)$ describes the geometry of the spiral pattern (*locus*), given by Roberts, Huntley & van Albada (1979), as

$$g(R) = -\frac{2}{N \tan i_p} \ln[1 + (R/R_s)^N], \quad (2)$$

where i_p is the pitch angle, R_s is the start position for the spiral arms, and N is a constant that

shapes the starting point of the spiral arms, **so that** $N \rightarrow 0$ represents a 180° tip transition from the bar to the spiral arms, while $N \rightarrow \infty$ means a 90° tip transition from the bar to the spiral arms. In the present work, we set it equal to 100 (for further details, see Pichardo et al. 2003).

2.1.2 PERLAS model

In contrast, the PERLAS spiral arms model (Pichardo et al. 2003) is a bisymmetric, three-dimensional, self-gravitating stationary model based on an adjustable mass distribution, rather than a local arm approximation, as the cosine potential. Several studies have shown that there are differences in the stellar orbital dynamics when the spiral arms are modeled with the cosine potential or with the PERLAS model (Pichardo et al. 2003; Antoja et al. 2009, 2011). Furthermore, chaotic orbital studies have demonstrated that a more detailed spiral arm potential (e.g., the PERLAS model) induces an important fraction of chaos, enough to destroy the spiral structure (Pérez-Villegas et al. 2013, 2012), when all chaotic behavior was originally attributed to effects produced by the bar, such as overlapping of resonances (Contopoulos & Harsoula 2012; Contopoulos 1967).

PERLAS is constructed by a superposition of individual oblate inhomogeneous spheroids along a given locus (the same than in the cosine potential, equation 2) and superimposed to the axisymmetric background. In this model, the spiral arms have a well defined mass, unlike the cosine potential, where the spiral arms are treated as a periodic function of the potential not straightforward translatable to mass. The mass assigned to build the spiral arms in the PERLAS model is subtracted from the disk mass. Thus, the inclusion of PERLAS to the Galactic model does not modify the total mass of the original axisymmetric background. In Table 1 we present the parameters of spiral arms that we used in our simulations. For further details about the PERLAS model, we refer the reader to Pichardo et al. (2003).

2.2 Force fitting

In order to compare PERLAS with the cosine potential, we need to fit the spiral arm strength to make them as similar as possible. We achieve this by adjusting the amplitude of the cosine potential (the factor A in eq. 1) so that the resulting

Table 1. Parameters of the Galactic Model

| Parameter | Value | Reference |
|--------------------------------|--|--------------------|
| <i>Axisymmetric Components</i> | | |
| R_0 | 8.5 kpc | 1 |
| Θ_0 | 220 km s ⁻¹ | 1 |
| Bulge mass | $1.41 \times 10^{10} M_\odot$ | 1 |
| Disk mass | $8.56 \times 10^{10} M_\odot$ | 1 |
| Halo mass | $8.002 \times 10^{11} M_\odot$ | 1 |
| <i>Spiral Arms</i> | | |
| Locus | Logarithmic | 2, 3 |
| Arms number | 2 | 4 |
| Pitch angle(i) | $15.5 \pm 3.5^\circ$ | 4 |
| M_{arms}/M_{disk} | 0.03 ± 0.02 | 3 |
| Mass | $2.7 - 5.4 \times 10^9 M_\odot$ | 3 |
| Inner limit | 3.3 kpc | ILR position based |
| Outer limit | 12 kpc | CR position based |
| Scale-length | 2.5 kpc | Disk based |
| Pattern speed (Ω_P) | $-20 \text{ km s}^{-1} \text{ kpc}^{-1}$ | 5 |

References —(1) Allen & Santillán 1991; (2) Grosbøl, & Patsis 1998; (3) Pichardo et al. 2003; (4) Drimmel 2000; (5) Martos et al. 2004.

radial and azimuthal forces approximate the ones obtained using the PERLAS model.

Figures 1 and 2 show the resulting fit for the case of a Milky Way-like galaxy, where the pitch angle is 15.5° and spiral arm mass (in PERLAS) is 3% of the disk mass. In this case, the cosine amplitude A is $650 \text{ km}^2 \text{ sec}^{-2} \text{ kpc}^{-1}$. In Figure 1, each panel represents different radial lines, starting in 0° up to 75° . In the Figure 2, each panel shows the computed azimuthal force at different radii, from 4 to 10 kpc. Continuous lines represent PERLAS, dotted lines represent our fit to the cosine potential.

2.3 Spiral arm strength

The spiral strength is related to the pitch angle and the mass of the arm. In the PERLAS model, the spiral arm mass is a small fraction of the disk mass. To quantify the strength of the spiral arms, we calculated the $Q_T(R)$ parameter (Sanders & Tubbs 1980; Combes & Sanders 1981), frequently used to quantify the strength of bars and spiral arms (Buta & Block 2001; Laurikainen & Salo 2002). The value of $Q_T(R)$ is given by

$$Q_T(R) = \frac{F_T^{\max}(R)}{|\langle F_R(R) \rangle|}, \quad (3)$$

where $F_T^{\max} = |(\partial\Phi(R, \theta)/\partial\theta)/R|_{\max}$ represents the maximum amplitude of the tangential force at radius R , and $\langle F_R(R) \rangle$, is the average axisymmetric radial force. Figure 3 shows $Q_T(R)$ for the PERLAS (solid line) and cosine (dotted line) potential models, for the case where the spiral arms mass of the PERLAS model has a 3% of the disk mass.

As opposed to Figures 1 and 2, where the force amplitude is almost the same, Figure 3 shows that there is a difference between both potentials. While the maximum value of Q_T for PERLAS is ~ 0.096 , for cosine is only ~ 0.035 . Therefore, if the arm strength is measured using equation (3) instead of the arm force, it is necessary to increase the cosine model amplitude. Figure 4 shows the Q_T parameter corresponding to an increased cosine amplitude, in this case, $A = 2000 \text{ km}^2 \text{ sec}^{-2} \text{ kpc}^{-1}$. In this case, since Q_T for the cosine model is larger than PERLAS along all the radial range, this case should be considered as an example to test the gaseous disk response to an extreme cosine model, in order to verify if at this forcing the cosine can reproduce what PERLAS does. In this way we are bracketing the cosine potential within the values of the force for the PERLAS model.

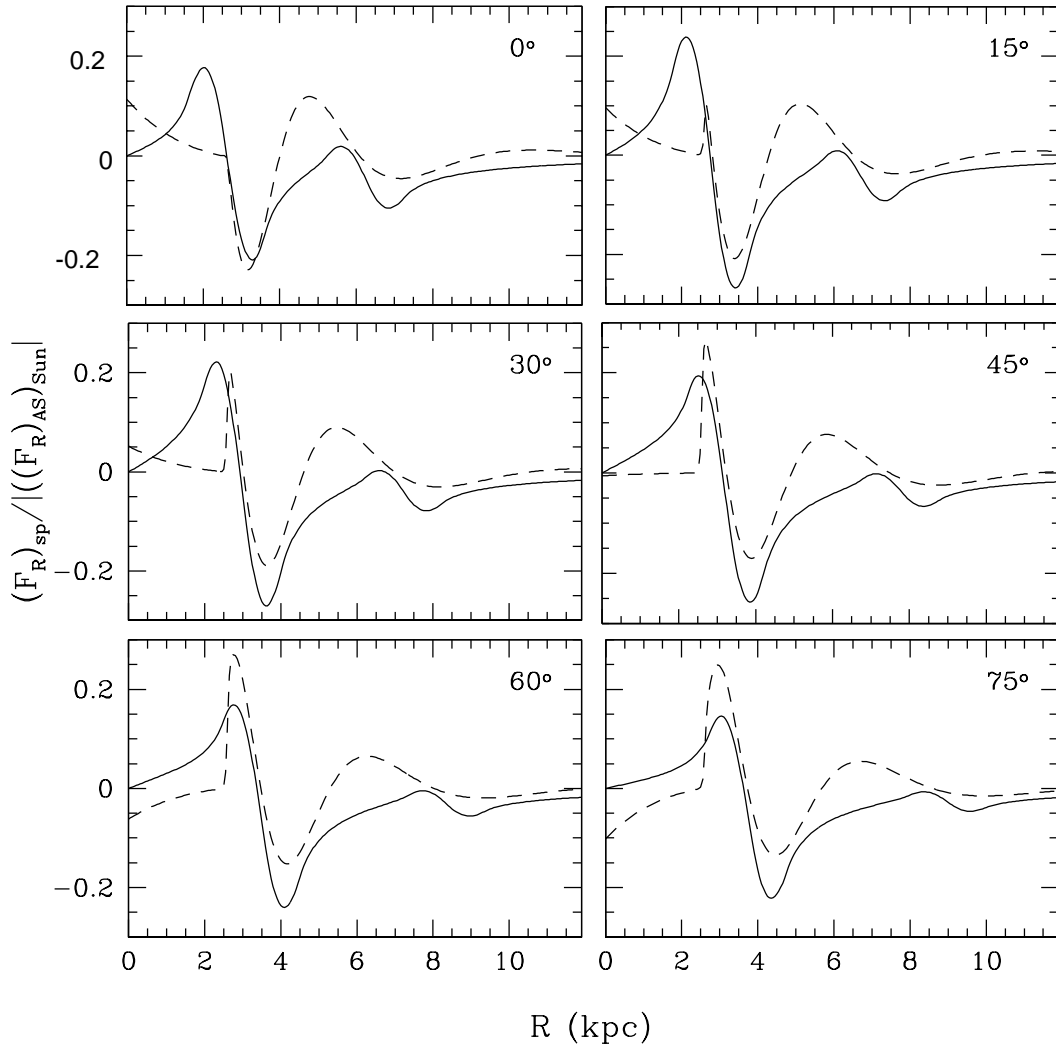


Figure 1. Radial force of the spiral arms along of the different radial lines, starting in 0° up to 165° , each 15° . The radial force is scaled to the axisymmetric background radial force at the solar position. Continuous lines represent PERLAS, dotted lines represent the best fit with equation 1.

2.4 The MHD set-up

The initial set-up of the simulations consisted on a gaseous disk, with density profile given by $n(r) = n_0 \exp[-(r-r_0)/r_d]$, where $n_0 = 1.1 \text{ cm}^{-3}$, $r_0 = 8 \text{ kpc}$ and $r_d = 15 \text{ kpc}$. The gas follows an isothermal equation of state with temperature $T = 8000 \text{ K}$. Additionally, the gas is permeated by a magnetic field, initially in the azimuthal direction, with an intensity given by $B(r) = B_0 \exp[-(r-r_0)/r_B]$, where $B_0 = 5 \mu\text{G}$

and $r_B = 25 \text{ kpc}$. The disk is set up in rotational equilibrium between the centrifugal force, the thermal and magnetic pressures, magnetic tension and the background axisymmetric potential (Allen & Santillán 1991). This equilibrium is perturbed by the spiral arm potentials under study, both rotating with a pattern speed $\Omega_p = 20 \text{ km s}^{-1} \text{ kpc}^{-1}$.

We employed the ZEUS code (Stone & Norman 1992a,b) to solve the MHD

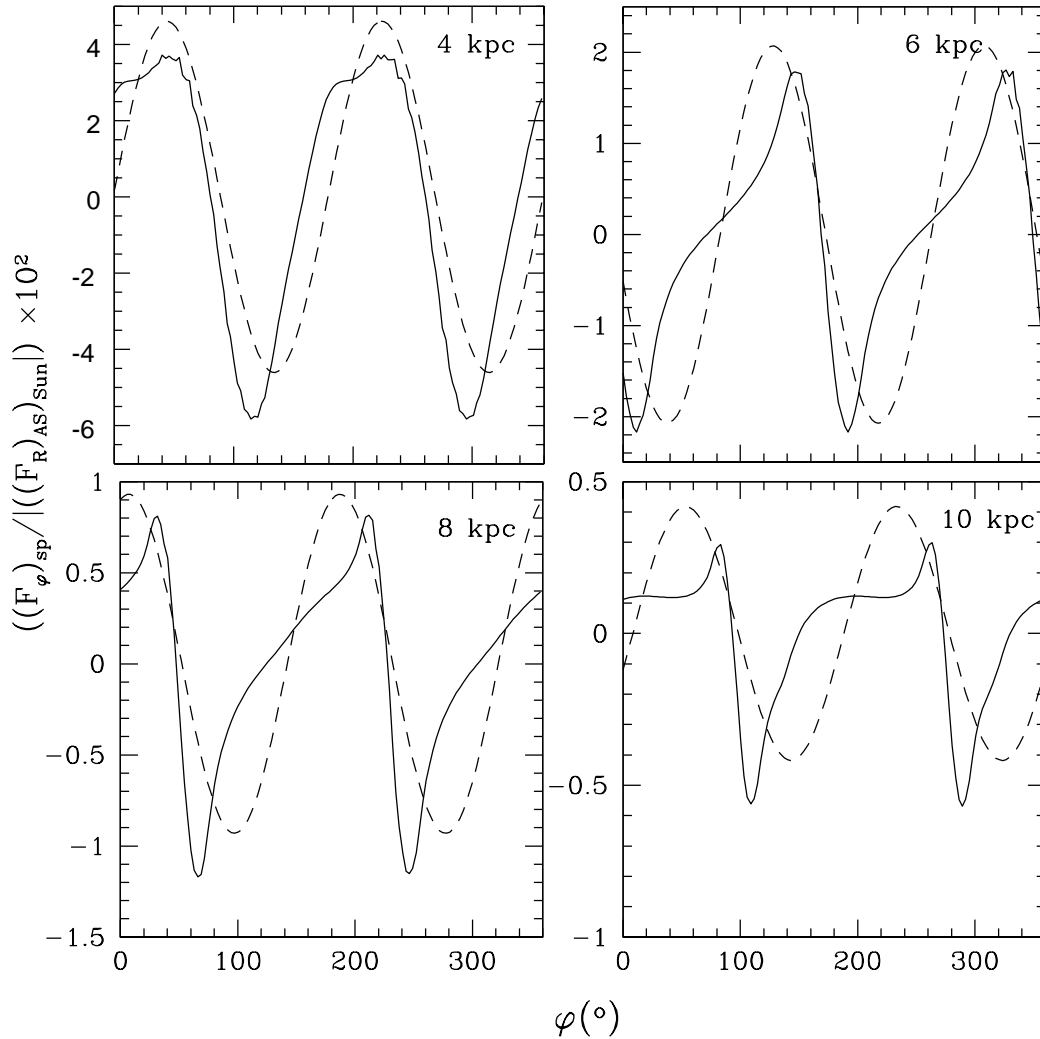


Figure 2. Azimuthal force at the different radius, from 4 to 10 kpc, each 2 kpc. The radial force is scaled to the axisymmetric background radial force at the solar position. Continuous lines represent PERLAS, dotted lines represent our fit with equation 1.

equations, which is a finite difference, time explicit, operator split, Eulerian code for ideal MHD. We used a 2D grid in cylindrical geometry, with $R \in [1.5, 22]$ kpc and a full circle in the azimuthal coordinate, ϕ , using 750×1500 grid points. Both boundary conditions in the radial direction were outflowing. All calculations are performed in the reference frame of the spiral arms. No self-gravity of the gas was considered.

3 RESULTS

We present in this section a comparison between the gas response to the simplified cosine potential for the spiral arms, and the density distribution based model PERLAS. In the limit for weak and/or small pitch angles (approximately linear regime), both models behave very similar as expected, however, for stronger arms (more massive or larger pitch angles), from this comparison we find severe differences in the gas behavior and for-

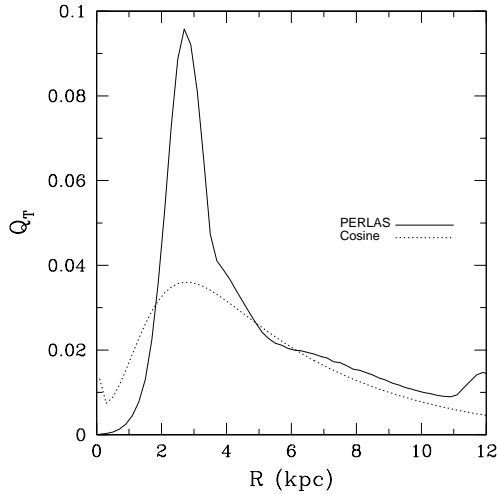


Figure 3. $Q_T(R)$ parameter for the spiral arms of a Milky Way-like galaxy for the PERLAS (*solid line*) and cosine (*dotted line*) potential models.

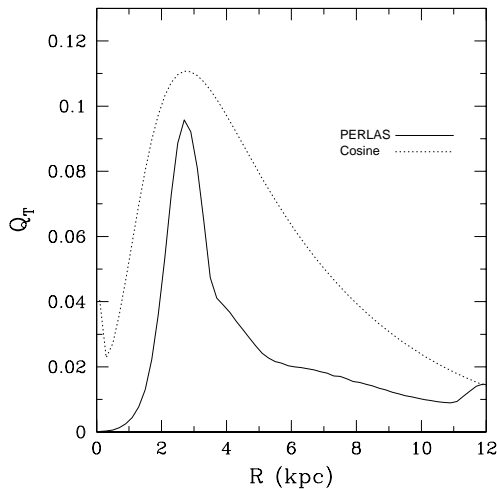


Figure 4. Similar to fig. 3, with the amplitude of the cosine model increased.

mation of spiral arms and branch-like structures. The deviation of the response between both models is induced by the basic differences of these potentials. We then present an interpretation on the presence of galactic branches prior to the ultra-

harmonic 4:1 resonance and connect them to a possible signature of transient spiral arms.

3.1 Gas Response Comparison: PERLAS vs. cosine Potential Models

In order to compare both potentials, we fit the cosine potential with PERLAS to make it as similar as possible in the force amplitude (§2.2). In all cases, the axisymmetric gaseous disk, initially in rotational equilibrium, was perturbed by the spiral potential either PERLAS or the cosine.

As mentioned already, the cosine potential represents a simple solution from the density wave linear theory, self-consistent for tightly wound spiral arms (TWA, i.e. where the perturbation is very small, which means small pitch angles or with very reduced masses). The Milky Way Galaxy and the most of spiral galaxies are actually far from this regime. Thus, it should not be surprising that the gaseous disk (Gómez et al. 2013) and the stellar orbits (Pérez-Villegas et al. 2012) show a different structure when subjected to a self-gravitating, more realistic model instead of a local approximation. With this in mind, the gaseous disk response to both models should be similar if we focus on a region of the parameter space where both potentials are valid, i.e., if we set PERLAS and the cosine potential so that it is approximately in the linear regime, with a very small pitch angle and spiral arm mass. In Figure 5 we show the linear regime for both potentials. The density distribution with the cosine potential is presented in the left panel and PERLAS model in the right panel, the pitch angle is 6° , the spiral arms mass is 1% of the disk mass, $A = 100 \text{ km}^2 \text{ s}^{-2} \text{ kpc}^{-1}$. Indeed, the gas response to the potentials is similar as expected, forming two spiral arms in both cases.

For the specific case of a Milky Way-like galaxy, we constructed a model that reproduces some of the observational parameters for the background and spiral arms potential to compare them with the cosine potential for the spiral arms (force fitted with PERLAS). The spiral arms pattern angular speed is $20 \text{ km s}^{-1} \text{ kpc}^{-1}$, on a logarithmic locus with a pitch angle of 15.5° . The mass of spiral arm for PERLAS model is 3% of the disk mass, which is equivalent to a cosine amplitude of $A = 650 \text{ km}^2 \text{ sec}^{-2} \text{ kpc}^{-1}$, when the non-axisymmetric force is employed for the fitting (see §2.2), and $A = 2000 \text{ km}^2 \text{ sec}^{-2} \text{ kpc}^{-1}$, when the arm strength (i.e. the Q_T parameter) is

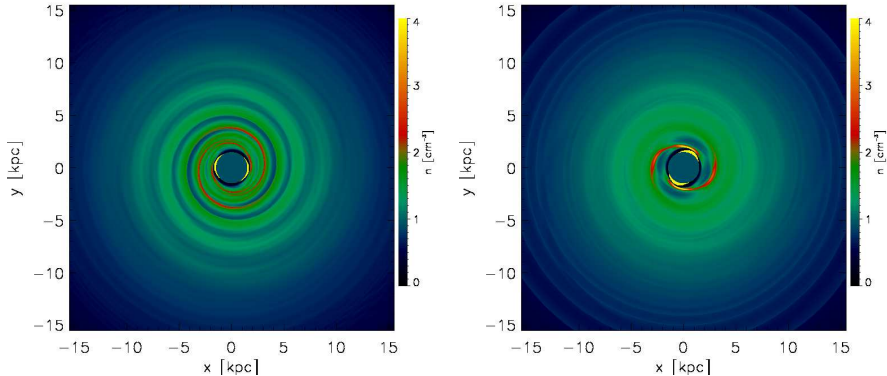


Figure 5. Density distribution for the simulation with the cosine potential (*left panel*) and with the PERLAS model in the linear regime (*right panel*) after 1.2 Gyr. In both cases, the pitch angle is 6° . The amplitude for the cosine potential is $A = 100 \text{ km}^2 \text{ sec}^{-2} \text{ kpc}^{-1}$ and the spiral arm mass for the PERLAS model is 1% of the stellar disk mass.

considered for the fitting instead (see §2.3). We **follow the evolution of the system** for 5 Gyr.

Figure 6 shows the resulting density distribution of the gaseous disk when is perturbed by the cosine potential with a small amplitude ($A = 650 \text{ km}^2 \text{ sec}^{-2} \text{ kpc}^{-1}$). After the simulation starts, the gas very rapidly settles into a spiral pattern, forming two spiral arms at 30 Myr (top left panel). 300 Myr into the simulation (top right panel), the two spiral arms are better defined, and the gas is forming a secondary structure. As simulation progresses (1.5 and 3 Gyr, bottom panels), the gas continues responding to the spiral arms and even more substructure forms, but the large scale density response consists of two arms only. The pitch angle of the formed arms is $\sim 15.5^\circ$, equal to the imposed potential at the beginning of the simulation. In the last panel, a gas instability at the corotation radius is seen, as reported previously (Gómez et al. 2013; Martos et al. 2004).

In contrast, Figure 7 shows the density distribution of the gaseous disk when is perturbed by the PERLAS spiral arm potential. The gas very rapidly settles into a spiral pattern, as in the cosine potential case, forming two spiral arms at 30 Myr. At 300 Myr and later, the gas forms four spiral arms instead of the two arms in the cosine potential simulation. Even though the simulation develops four spiral arms, these are associated in two **pairs, each composed of** a strong arm and a weak arm. The strong arms have a pitch angle of $\sim 15^\circ$, and the weak arms have a pitch angle

of $\sim 7^\circ$. This doubling of the spiral arms in the gas response has been seen in other MHD simulations using the PERLAS model (Gómez et al. 2013; Martos et al. 2004; see also §3.2).

In §2.3, we noted that the spiral arm strength, as measured by eq. (3), was very different for both potentials, even if the force amplitudes were almost the same. Therefore, we decided to perform a second experiment with a larger amplitude $A = 2000 \text{ km}^2 \text{ sec}^{-2} \text{ kpc}^{-1}$ for the cosine potential, that would be equivalent to a factor of ~ 3 times the force of PERLAS. This much larger amplitude for the cosine potential is stronger than PERLAS at any radii, as shown in Figure 4. The purpose of this overestimated experiment was to test if the four spiral arms formed with PERLAS were due to the strength of spiral arms only. Figure 8 shows the gas density distribution resulting from perturbing the disk with the larger force amplitude of the cosine potential. It is readily seen that the effect of the spiral potential on the gas disk is larger and generates more substructure, but the gas still responds forming two spiral arms, unlike the density based potential PERLAS that forms four arms for larger pitch angles, i.e. for stronger arms. Consequently, this difference does not come from the force amplitude, but it seems rather originated from the self-gravitating nature and specific details of the potential that a local approximation for the forces given by the cosine potential is unable to reproduce. We further explain this in the next section.

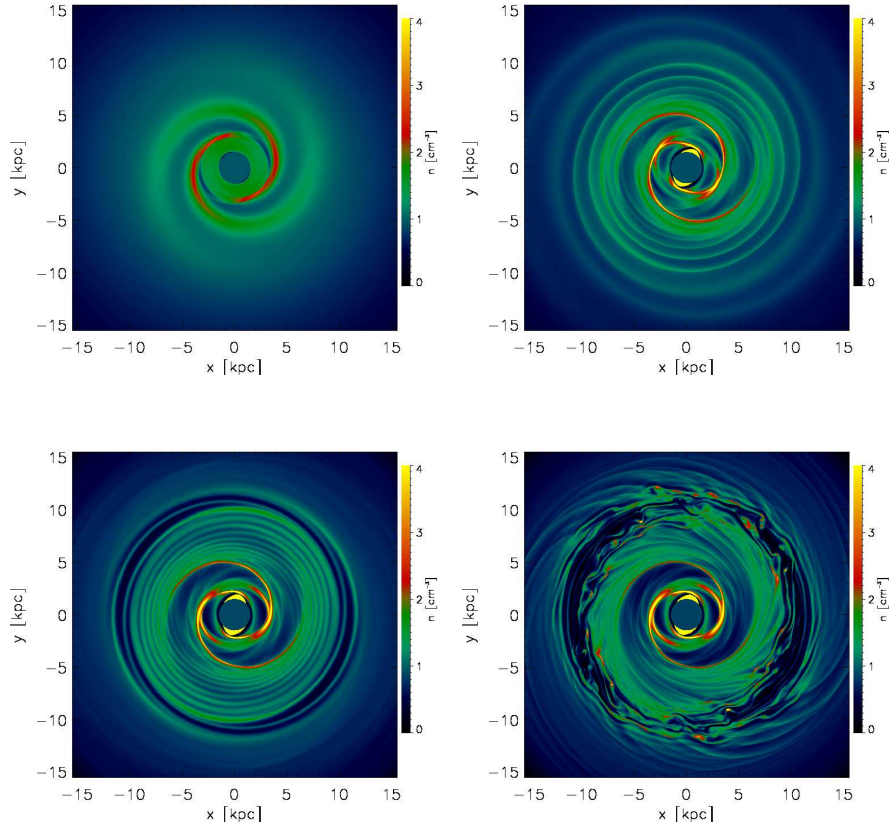


Figure 6. Density distribution using a cosine potential to model spiral arms. Times shown in this plot correspond to 30 Myr after the simulation starts (*top left panel*), 300 Myr (*top right panel*), 1.5 Gyr (*bottom left*), and 3 Gyr (*bottom right*).

3.2 Branch Formation and their Relation with the Transient Nature of Spiral Arms

In §3.1 we showed that the intrinsic differences in the nature of the cosine and PERLAS potentials induce a distinct gaseous arm structure as compared to a disk perturbed by a cosine arm potential. While employing the spiral arm cosine potential, a bisymmetric gaseous structure seems to be an invariable outcome, for the PERLAS potential a two or four armed structure could be obtained. This result points to the necessity of understanding how the gas responds to the PERLAS model when we vary the structural parameters of the spiral arms, such as its mass and pitch angle, considering the uncertainties in the determination of these parameters for the Milky Way’s

spiral arms. Therefore, we developed a set of simulations varying spiral arm pitch angles (i) and spiral arms masses. We present here some of them ranging from 12° to 19° , and the mass of the spiral arms (M_{sp}), from 1.75% to 5% of the total disk mass (M_D).

Figure 9 shows a mosaic of simulations. The panels in the left column are the stable periodic stellar orbits and the panels in the right column are the gas density distribution after 1.2 Gyr. **The maximum density response (where the orbits crowd producing a density enhancement) quantifies the orbital support to a given spiral perturbation through periodic orbits. We computed the stellar periodic orbits in order to explore the orbital support to the imposed PERLAS spiral arm potential (open squares in**

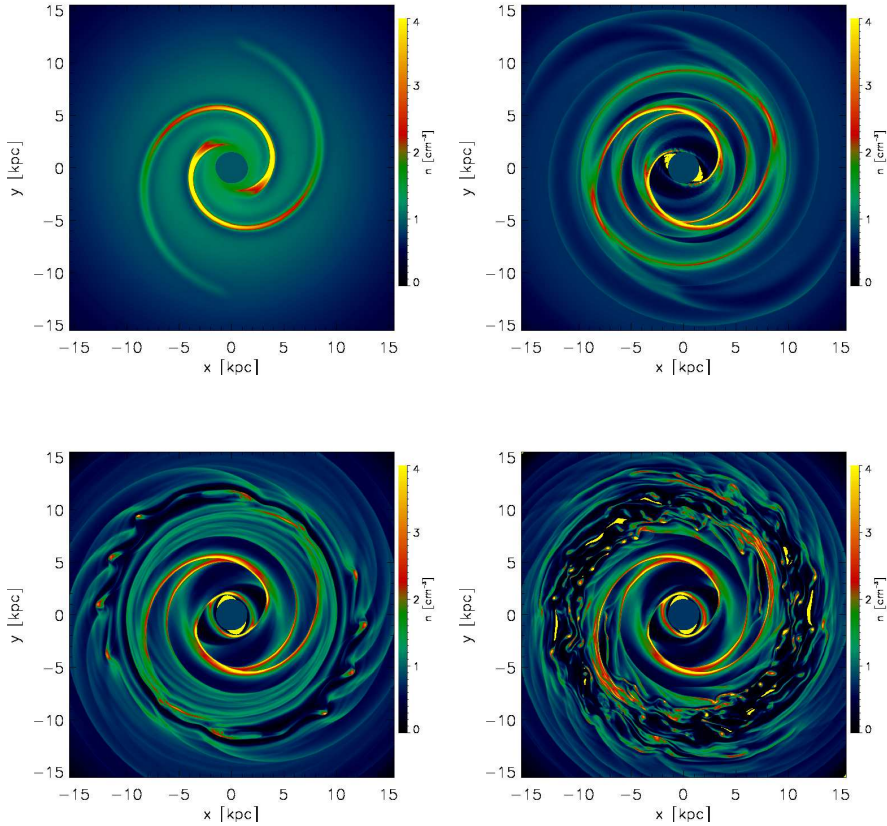


Figure 7. Density distribution using the PERLAS spiral arm model. Panels correspond to the same evolution times as in fig. 6

the left column-panels of Figure 9). To estimate the density response, we employ the method of Contopoulos & Grosbøl (1986). This method assumes that stars in circular orbits in an axisymmetric potential, with the same sense of rotation of the spiral arms, are trapped around the corresponding periodic orbit in the presence of the spiral arms. For this purpose, we calculated a set of central periodic orbits (between 50 and 60) and found the density response along them using the conservation of the mass flux between any two successive periodic orbits. With this information we seek the position of the maximum density response along each periodic orbit (filled squares in the left column-panels of fig. 9). These positions are compared with the imposed spiral

arms (PERLAS model). The method implicitly considers a small dispersion (with respect to the central periodic orbit) since it studies a region where the flux is conserved. On the other hand, this dispersion is based on parameters for the galaxies where dynamics is quite ordered, orbits follow their periodic orbit closely, in such a way that we consider this study a good approximation. This method to estimate the density response has been widely used in literature (Contopoulos & Grosbøl 1988; Amaral & Lepine 1997; Yano et al. 2003; Pichardo et al. 2003; Voglis et al. 2006; Tsoutsis et al. 2008; Pérez-Villegas et al. 2012, 2013; Junqueira et al. 2013). We refer the reader to the work of Contopoulos & Grosbøl (1986) for more details. With this in mind, a model in

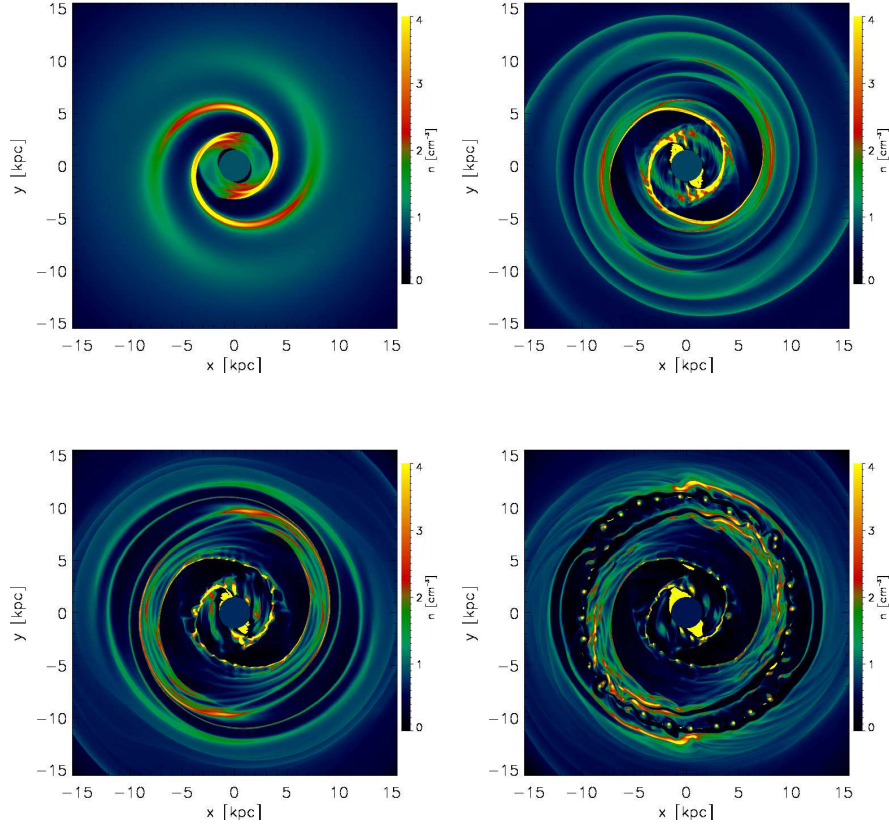


Figure 8. Gas density distribution for the simulation with the cosine potential when its force amplitude is increased by a factor of ~ 3 (up to the value provided by PERLAS model). The times shown correspond to 30 Myr (top left panel), 300 Myr (top right panel), 900 Myr (bottom left panel), and 1.5 Gyr (bottom right panel).

Figure 9 where the open and filled squares coincide would represent a stable, approximately orbitally self-consistent system, while a lack of coincidence would mean that the spiral is unlikely to be long-lasting (Pérez-Villegas et al. 2012, 2013).

For $M_{sp} = 0.0175M_D$ and $i = 12^\circ$ (upper left panel of Figure 9), the stellar density response follows approximately the imposed spiral potential prior to the 4/1 resonance. After that, the stellar response forms a slightly smaller pitch angle than the imposed spiral. In the MHD simulation, the gaseous disk responds to the two-arm potential with the now familiar four spiral armed structure, where the pitch angle of the stronger pair of arms corresponds to that of the imposed pitch angle potential, while the other pair of gaseous arms has a systematically smaller pitch angle, corre-

sponding closely to the regions of periodic orbits crowding. Now, with the same spiral arm mass but a pitch angle of $i = 19^\circ$ (second row of fig. 9), the stellar density response (i.e. periodic orbits) forms again a smaller pitch angle compared with the imposed, while in the gas, the four spiral arms seem stronger and the difference in the pitch angle between the gaseous and imposed arms is larger than the previous case. For $M_{sp} = 0.05M_D$ and $i = 12^\circ$ (third row), the stellar density response closely follows the imposed spiral arm potential prior to the 4/1 resonance. After that, the stellar response forms a slightly smaller pitch angle than the imposed spiral, while the gas responds with four spiral arms, but the second pair is very weak but with a significantly smaller pitch angle than the imposed spiral arm potential. Finally, with the same spiral arm mass (5% of the disk

mass) but a pitch angle of $i = 19^\circ$ (fourth row), we found no periodic orbits beyond 4/1 resonance and the stellar density response forms a pitch angle smaller than 19° . The gaseous disk responds with well defined four spiral arms that extend up to the corotation radius. Notice that in this last simulation, there is not much that can be said about the (stellar or gaseous) orbital support since periodic orbits tend to disappear due to the strong forcing of the imposed spiral arms, meaning that spiral arms would rather be transient by construction in this case and the MHD gaseous disk behavior is difficult to predict from periodic orbit computations. However, such as the stellar arms constructed in this case, the gaseous spiral would be transient in likely even shorter timescales than in the case where periodic orbits exist but settle down systematically in smaller pitch angles than the original imposed spiral arms in the region where periodic orbits do exist. Notice that, in general, the arms that should eventually disappear in this scenario, are the stronger stellar imposed spiral arms (see second row of fig. 9; Pérez-Villegas et al. 2013).

Therefore, the stellar response density maxima represent the regions of the arms where stars would crowd for long timescales, this is, where the existence of stable, long-lasting spiral arms would be more likely. On the other hand, if the stellar density response forms a spiral arm with a different pitch than the imposed angle, then the imposed spiral arms triggered on the disk (by a bar, an interaction, etc.), would rather be structures of transient nature since those are not orbitally supported (Pérez-Villegas et al. 2013). Likewise, for the case of the spiral arms in the Milky Way, the values frequently seen in literature for the pitch angle, range from $\sim 11^\circ$ to 19° . These values and the knowledge of the galactic type could provide some information about their nature, i.e. whether they are long-lasting or transient structures. **Following the pitch angle restrictions found by Pérez-Villegas et al. (2013), the larger pitch angle values reported in literature for the Milky Way galaxy would imply that its spiral arms are a transient feature.** The formation of four spiral arms in the gas response is, in this scenario, another piece of evidence of a transient nature of the spiral arms in the Milky Way galaxy, as we claim it is the secondary pair of arms in Figure 9, that coincides **more** closely with the stellar density response **from** periodic orbits, as expected from Gómez et al. (2013).

Summarizing, the first (imposed) pair of massive spiral arms formed in the disk, with a larger pitch angle, triggers a second pair of arms (traced approximately by the periodic orbits), with smaller pitch angles (Pérez-Villegas et al. 2013). In this outline, the gas responds forming a second pair of arms aligned with the locus of the orbital crowding. This lighter structures would likely be preferentially formed by young stars and gas than by evolved stars because of their transient nature, i.e. similar to what we call “branches”. Finally, in this framework, the presence of clear and strong branches in spiral galaxies, with smaller pitch angles than the corresponding couple of massive spiral arms on a galaxy, would be a signature of the transient nature of the spiral arms in a given galaxy. On the other hand, spiral galaxies without evidence of branches could indicate the presence of a longer lasting spiral arm structure.

4 DISCUSSION AND CONCLUSIONS

With the use of a detailed three dimensional, density-distribution based potential for the spiral arms, combined with MHD simulations on a Milky Way-like galactic disk, we have studied the stellar orbital and gaseous response to the galactic potential. As a first experiment, we constructed a simple cosine potential (as the ones commonly employed in literature) that reproduced approximately what the density based potential PERLAS exerts on the stellar and gaseous dynamics.

The first set of simulations compare the gas response when the disk is perturbed by both spiral arm potential models. We also varied the structural parameters of the spiral arms in the PERLAS model, such as the pitch angle (12° to 19°) and the mass of spiral arms (1.75% to 5% of the stellar disk mass) in order to understand how these parameters affect the gaseous disk dynamics. Additionally, we constructed stellar periodic orbits and calculate the stellar response density maxima.

With these exercises we found that only in the case of the PERLAS model the gas and stellar density response (based on the existence of periodic orbits) is a consistent four-armed spiral structure: a couple of strong gaseous arms located at the position of the imposed stellar arms, and a second pair of weaker gaseous arms located at the position of the stellar orbit crowding. **Since the potential and the stellar density response**

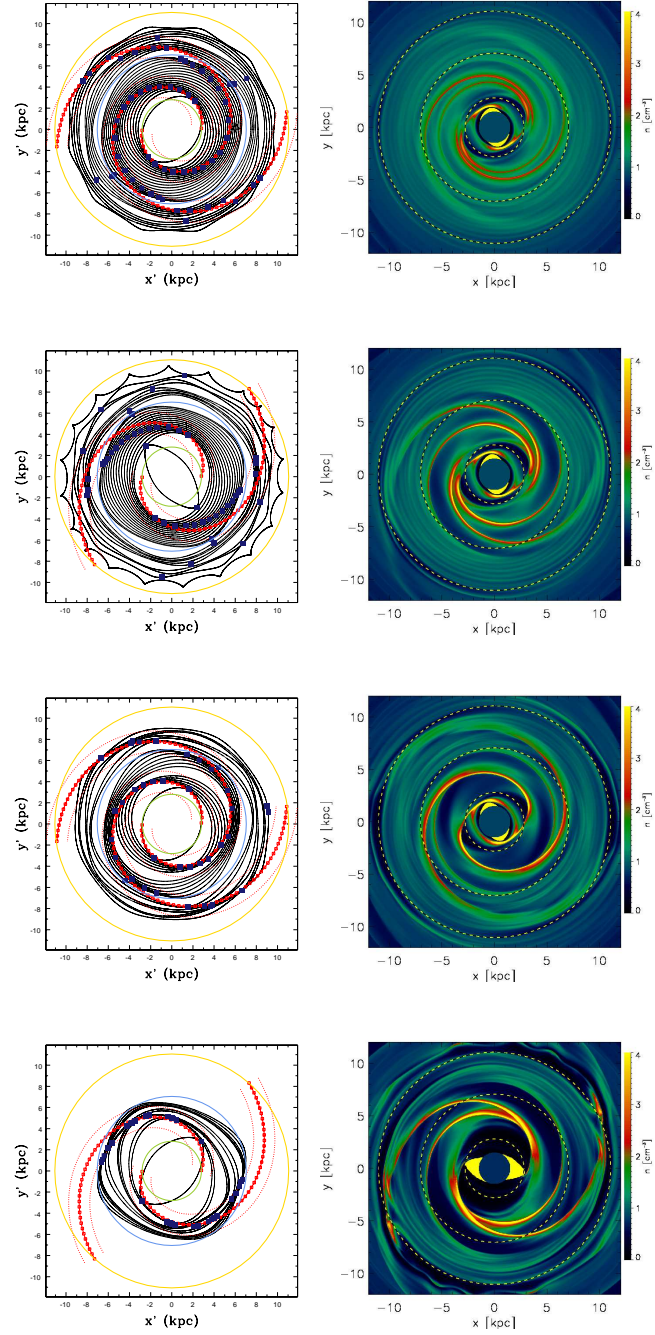


Figure 9. Stellar and gaseous response to different parameters of the spiral arm model (PERLAS). Panels on the left column show the stable periodic stellar orbits (*black solid lines*), the response density maxima (*filled squares*), and the imposed spiral arm locus (*open squares*), flanked by two dotted lines that represent the spiral arm width. Colored circles represent the position of the inner Lindblad (*green*), 4/1 (*blue*) and corotation (*yellow*) resonances. Panels on the right column show the gas density distribution after 1.2 Gyr, together with the inner Lindblad, 4/1 and corotation resonances (*dashed circles*). The mass of spiral arms and pitch angle are: $M_{sp} = 0.0175M_D$ with $i = 12^\circ$ (*first row*) and $i = 19^\circ$ (*second row*), $M_{sp} = 0.05M_D$ with $i = 12^\circ$ (*third row*) and $i = 19^\circ$ (*fourth row*).

do not coincide, the spiral arms are prone to destruction. So, the presence of the second (gaseous) pair is interpreted as a sign of this transiency.

Our main conclusions can be summarized as follows:

- **We performed a study of the gas response to two galactic potentials: the density distribution based model PERLAS and the widely employed in literature cosine potential. We verified that the gas response (a two armed structure) is the same for both models close to the linear regime only, i.e. for low-mass spiral arms and pitch angles smaller than $\sim 10^\circ$.** In the general case however (i.e. large pitch angle or arm mass), even when the cosine potential has been fitted as close as possible to the PERLAS model, they produce quite distinct outcomes on the gas response. In the case of the cosine potential, the gas responds invariably forming two spiral arms while, with the PERLAS model, the gas responds with four gaseous spiral arms (in the general strong arm case).

- We increased the strength of the spiral arms represented by the cosine potential up to a point the arms were equivalent and even beyond the mass of a strong bar as an experiment to try to reproduce the gas response provided by the PERLAS model. However, the answer was always a bisymmetric structure. We conclude that the spiral arm strength is not responsible for the four-arm gas response, but rather it is the product of the forcing generated by the whole density distribution better represented by the PERLAS model that, in turn, forces the periodic orbit response to shift its crowding regions inside the imposed locus of the massive spiral arms.

- Using the PERLAS model, we changed the structural parameters of the spiral arms according to the observational and theoretical uncertainties in the determination of the Milky Way's spiral arms in literature. Within these values, for the general case, the stellar response density maxima systematically forms spiral arms with a smaller pitch angle than the imposed spiral, meaning that the spiral arms might be a transient feature in the Milky Way Galaxy (Pérez-Villegas et al. 2013). The presence of a second pair of lighter spiral arms (“branches”), with smaller pitch angles induced by the first more massive stellar spiral arms, might be evidence of the lack of support to the stronger arms on a galactic disk, and therefore evidence of the

transient nature of spiral arms in a given galaxy. Applying this scenario to the Milky Way, for the stronger spiral arm values reported in literature (i.e. pitch angles larger than $\sim 10^\circ$, and masses larger than $\sim 2\%$ of the disk), the spiral arms in the Milky Way would be of transient nature.

- Although in this work we applied the models to Milky Way-like galactic discs, it is worth noticing that the results are general. This means that the presence of branches with smaller pitch angles than the main arms might be the “smoking gun” that proves transiency of spiral arms in any given galaxy.

ACKNOWLEDGMENTS

We thank Edmundo Moreno for enlightening discussions that helped to improve this work. APV acknowledges the support of the postdoctoral Fellowship of DGAPA-UNAM, México. This work has received financial support from DGAPA PA-PIIT grants IN111313 and IN114114.

REFERENCES

- Allen, C. & Santillán, A. 1991, *Rev. Mexicana Astron. Astrofis.*, 22, 256
- Amaral, L. H., & Lepine, J. R. D. 1997, *MNRAS*, 286, 885
- Antoja, T., Figueras, F., Torra, J., Valenzuela, O., & Pichardo, B. 2010, *Lecture Notes and Essays in Astrophysics*, 4, 13
- Antoja, T., Valenzuela, O., Pichardo, B., Moreno, E., Figueras, F. & Fernández D. 2009, *ApJ*, 700, L78
- Antoja, T., Romero-Gómez, M., Figueras, F., Valenzuela, O., Pichardo, B. & Moreno, E. 2011, *MNRAS*, 418, 1423
- Artymowicz, P., & Lubow, S. H. 1992, *ApJ*, 389, 129
- Balbus, S. A. 1988, *ApJ*, 324, 60
- Barbanis, B., & Woltjer, L. 1967, *ApJ*, 150, 461
- Bate, M. R., 1997, *MNRAS*, 285, 16
- Benjamin, R. A., Churchwell, E., Babler, B. L., et al. 2005, *ApJ*, 630, L149
- Buta, R. & Block, D. L., 2001, *ApJ*, 550, 243
- Chakrabarti, S., Laughlin, G., & Shu, Frank H., 2003, *ApJ*, 596, 220
- Combes, F., & Sanders, R. H. 1981, *A&A*, 96, 164
- Contopoulos, G. 1967, *Bull. Astron. (Ser. 3)*, 2, 223

- Contopoulos, G. & Grosbøl, P., 1986, *A&A*, 155, 11
- Contopoulos, G. & Grosbøl, 1988, *A&A*, 197, 83
- Contopoulos, G., & Harsoula, M. 2012, *Celestial Mechanics and Dynamical Astronomy*, 113, 81
- Corder, S., Sheth, K., Scoville, N. Z., et al. 2008, *ApJ*, 689, 148
- Dobbs, C. L., & Bonnell, I. A. 2006, *MNRAS*, 367, 873
- Dobbs, C. L., Burkert, A., & Pringle, J. E. 2011, *MNRAS*, 417, 1318
- Donner, K. J., & Thomasson, M. 1994, *A&A*, 290, 785
- D’Onghia, E., Vogelsberger, M., & Hernquist, L. 2013, *ApJ*, 766, 34
- Drimmel, R. 2000, *A&A*, 358, L13
- Drimmel, R., & Spergel, D. N. 2001, *ApJ*, 556, 181
- Dwek, E., Arendt, R. G., Hauser, M. G., et al. 1995, *ApJ*, 445, 716
- Eden, D. J., Moore, T. J. T., Morgan, L. K., Thompson, M. A., & Urquhart, J. S. 2013, *MNRAS*, 431, 1587
- Elmegreen, D. M. 1980, *ApJ*, 242, 528
- Englmaier, P., & Gerhard, O. 1999, *MNRAS*, 304, 512
- Feitzinger, J.V., & Schwerdtfeger, H., 1982, *A&A*, 116, 117
- Foyle, K., Rix, H.-W., Walter, F., & Leroy, A. K. 2010, *ApJ*, 725, 534
- Foyle, K., Rix, H.-W., Dobbs, C. L., Leroy, A. K., & Walter, F. 2011, *ApJ*, 735, 101
- Fujimoto, M. 1968, *Non-stable Phenomena in Galaxies*, 29, 453
- Fux, R. 1999, *A&A*, 345, 787
- Gómez, G. C., Pichardo, B., & Martos, M. A. 2013, *MNRAS*, 430, 3010
- Grosbøl, P. J. & Patsis, P. A. 1998, *A&A*, 336, 840
- Junqueira, T. C., Lépine, J. R. D., Braga, C. A. S., & Barros, D. A. 2013, *A&A*, 550, AA91
- Kawata, D., Hunt, J. A. S., Grand, R. J. J., Pasetto, S., & Cropper, M. 2014, *MNRAS*, 443, 2757
- Kim, W.-T., Kim, Y., & Kim, J.-G. 2014, *ApJ*, 789, 68
- Kim, Y., & Kim, W.-T. 2014, *MNRAS*, 440, 208
- Kim, W.-T. & Ostriker, E. C., 2002, *ApJ*, 570, 132
- Kim, W.-T. & Ostriker, E. C., 2006, *ApJ*, 646, 213
- Laurikainen, Eija & Salo, Heikki, 2002, *MNRAS*, 337, 1118
- Lee, Wing-Kit & Shu, Frank H., 2012, *ApJ*, 756, 45
- Lin, C. C. & Shu, F. H., 1964, *ApJ*, 140, 646
- Lynds, B. T. 1970, *The Spiral Structure of our Galaxy*, *Proc. IAU Symp.* 38, 26
- Martínez-García, E. E., & González-Lópezlira, R. A. 2013, *ApJ*, 765, 105
- Martos, M., Hernandez, X., Yáñez, M., Moreno, E., & Pichardo, B. 2004, *MNRAS*, 350, L47
- Matsumoto, T., Hayakawa, S., Koizumi, H., et al. 1982, *The Galactic Center*, 83, 48
- Moore, T. J. T., Urquhart, J. S., Morgan, L. K., & Thompson, M. A. 2012, *MNRAS*, 426, 701
- Patsis, P. A., Hiotelis, N., Contopoulos, G., & Grosbol, P. 1994, *A&A*, 286, 46
- Patsis, P. A., Grosbol, P., & Hiotelis, N. 1997, *A&A*, 323, 762
- Pérez-Villegas, A., Pichardo, B., & Moreno, E. 2013, *ApJ*, 772, 91
- Pérez-Villegas, A., Pichardo, B., Moreno, E., Peimbert, A., & Velázquez, H. M. 2012, *ApJ*, 745, L14
- Pichardo, B., Martos, M., Moreno, E. & Espre-sate, J., 2003, *ApJ*, 582, 230
- Roberts, W. W. 1969, *ApJ*, 158, 123
- Roberts, W.W., Jr., Huntley, J. M., & van Al-bada, G. D., 1979, *ApJ*, 233, 67
- Roca-Fàbrega, S., Valenzuela, O., Figueras, F., et al. 2013, *MNRAS*, 432, 2878
- Roca-Fàbrega, S., Antoja, T., Figueras, F., et al. 2014, *MNRAS*, 440, 1950
- Roškar, R., Debattista, V. P., Quinn, T. R., & Wadsley, J. 2012, *MNRAS*, 426, 2089
- Sanders, R. H., & Tubbs, A. 1980, *AJ*, 235, 803
- Scarano, S., & Lépine, J. R. D. 2013, *MNRAS*, 428, 625
- Scoville, N. Z., Polletta, M., Ewald, S., et al. 2001, *AJ*, 122, 3017
- Sellwood, J. A. 2011, *MNRAS*, 410, 1637
- Sellwood, J. A., & Carlberg, R. G. 2014, *ApJ*, 785, 137
- Seo, W.-Y., & Kim, W.-T. 2014, *ApJ*, 792, 47
- Shetty, R., & Ostriker, E. C. 2006, *ApJ*, 647, 997
- Shu, F. H., Milione, V., & Roberts, W. W., Jr. 1973, *ApJ*, 183, 819
- Stone J. M., Norman M. L., 1992a, *ApJS*, 80, 753
- Stone J. M., Norman M. L., 1992b, *ApJS*, 80, 791
- Sofue, Y. 1976, *A&A*, 48, 1
- Tsoutsis, P., Efthymiopoulos, C., & Voglis, N. 2008, *MNRAS*, 387, 1264

- Vallée, J. P. 2002, *ApJ*, 566, 261
Vallée, J. P. 2013, *International Journal of Astronomy and Astrophysics*, 3, 20
Voglis, N., Stavropoulos, I. & Kalapotharakos, C. 2006, *MNRAS*, 372, 901
Wada, K., Baba, J., & Saitoh, T. R. 2011, *ApJ*, 735, 1
Wada, K., & Koda, J. 2004, *MNRAS*, 349, 270
Weiner, B. J., & Sellwood, J. A., 1999, *ApJ*, 524, 112
Weaver, H. F. 1970, *Interstellar Gas Dynamics*, IAU Symp. 39, 22
Yano, T., Kan-Ya, Y., & Gouda, N. 2003, *PASJ*, 55, 409
Yañez, Miguel A., Norman, Michel I., Martos, MArco A., & Hayes, John C., 2008, *ApJ*, 672, 207
Zhang, X. 1998, *ApJ*, 499, 93
Zhao, H. 1996, *MNRAS*, 283, 149